Results from H.E.S.S.

Werner Hofmann, for the H.E.S.S. collaboration
Max-Planck Institut für Kernphysik, Heidelberg

H.E.S.S. is new system of Cherenkov telescopes located in Namibia, which has been taking data with its first telescope since 2002, and with all four telescopes since late 2003. First H.E.S.S. results are reported, with emphasis on Galactic sources, such as supernova remnants and the Galactic Center.

1. Introduction: the H.E.S.S. instrument

Imaging atmospheric Cherenkov telescopes (IACTs) have emerged as the most powerful instruments for gamma-ray astronomy in the TeV regime. IACTs detect the Cherenkov light emitted by gamma-induced air showers, illuminating on the ground a circle of roughly 250 m in diameter, with a light density of about 100 photons/(m^2TeV) in the 300 nm to 600 nm wavelength range. A telescope mirror collects the Cherenkov light and images it onto a PMT 'camera' (Fig. 1). The intensity of the Cherenkov image provides a measure for the shower energy, the orientation of the shower image is related to the direction of the primary particle, and the shape of the images allows to separate the (well-collimated) gamma-induced electromagnetic air showers from the (more diffuse) cosmic-ray induced hadronic showers, which constitute a uniform background. The low intensity of the Cherenkov light implies that instruments can only observe at night; even scattered moonlight seriously impacts the performance. Good sites allow annual observation times of around 1000 hours per year.

H.E.S.S. is a stereoscopic telescope system, where four telescopes provide multiple views of the air shower and enable the precise reconstruction of the direction and impact point of the gamma ray. The telescopes are located on a square of 120 m side length – matched to the size of the Cherenkov light pool – and have a mirror area of 107 m^2 each (Fig. 2). The mirrors are segmented into 382 facets, which can be aligned under remote control [1, 2]. As for any single-mirror telescope, the point spread function degrades with increasing distance from the optical axis, but remains smaller than the PMT pixel size out to the edge of the field of view (Fig. 3). Telescopes are equipped with 960-pixel PMT cameras; each pixels covers 0.16° on the sky, for a total field of view of 5°. This large field of view – compared to other instruments – is important for the investigation of extended objects such as supernova remnants.

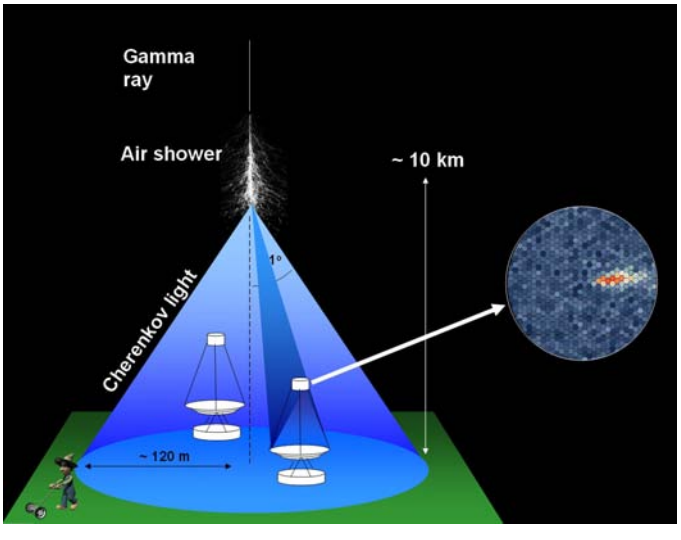

Figure 1: Detection of air showers with imaging atmospheric Cherenkov telescopes.

Figure 2: One of the four H.E.S.S. telescopes.

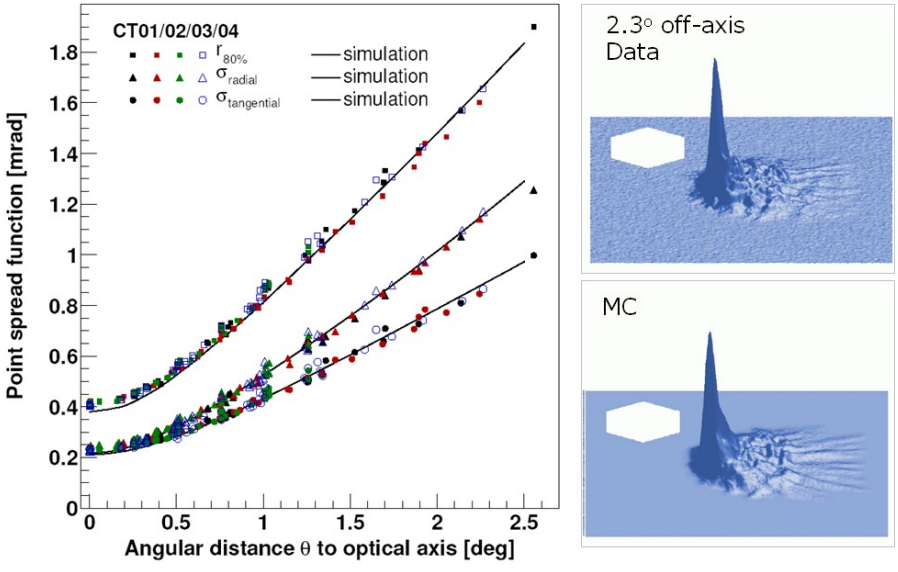

Figure 3: Left: point spread function of the reflectors of the H.E.S.S. telescopes, as function of the distance to the optical axis. All four telescopes behave identical. Right: Measured and simulated spot shapes, 2.3° off-axis, illustrating that the performance of the reflector is well-understood. The white hexagon indicates the size of the PMT pixels.

Unlike for other Cherenkov telescopes, the entire electronics is integrated into the camera body, eliminating signal transmission as a source of noise, bandwidth limitation, and cost [3]. PMT signals are sampled at 1 GHz using analog memories; upon a system trigger [4] (at least two telescopes see a shower), the digitized memory contents are sent to the central recording station, after some local processing. Communication between a telescope and the central station requires only a few optical fibers for the trigger and data links. Auxiliary instruments serve to monitor atmospheric conditions [5].

The dramatic improvement of the performance of Cherenkov instruments over the last decade is obvious if one

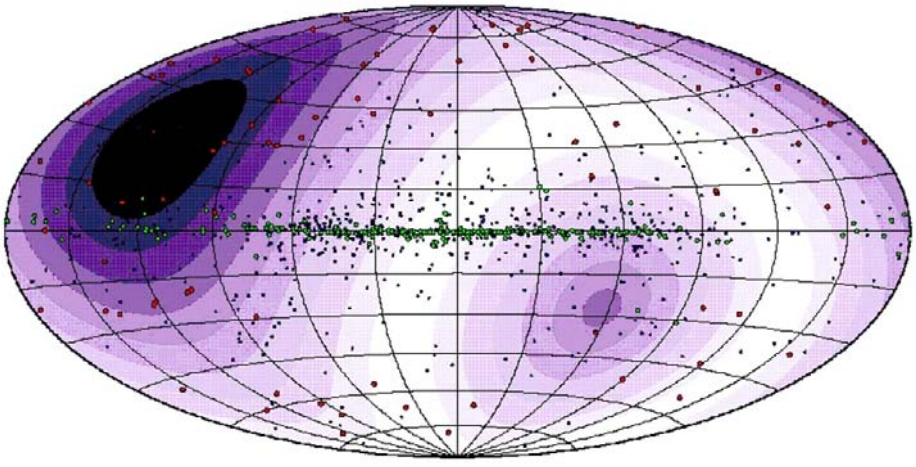

Figure 4: Sky coverage of H.E.S.S. in Galactic coordinates. Shades correspond to zenith angles at culmination; white regions imply optimal zenith angles, black regions are not visible to H.E.S.S. Symbols indicate interesting objects: pulsars (blue), supernova remnants (green), blazars (red).

recalls that in the mid-80's the Whipple telescope required about 50 h of observation time to achieve a 5σ signal from the Crab Nebula [6]; the HEGRA telescope system (1997-2002) [7] could detect the Crab Nebula within 15 min., and the H.E.S.S. system, with its energy threshold around 100 GeV, will see a source near zenith with the strength of the Crab within 30 sec.

The H.E.S.S. telescopes are located in Namibia, at $23°16'$ S $16°30'$ E. The southern location provides optimal viewing conditions for the central region of our Galaxy, with its large numbers of supernova remnants and pulsars as potential emitters of high-energy radiation (Fig. 4).

The first H.E.S.S. telescope began operation in Summer 2002; typical Cherenkov images are shown in Fig. 5. The muon rings are used to check the calibration of the telescopes; from the measured ring radius the expected number of photoelectrons can be predicted, and compared with the image intensity. Muon rings provide about half of the triggers of a single telescope. Once a coincidence between two or more telescopes is required, muon triggers are virtually eliminated [4]. In 2002 and 2003, the H.E.S.S. telescope system was still under construction; nevertheless, substantial amounts of data were accumulated with one, two or three telescope configurations (Fig. 6)

2. The Crab Nebula

In winter 2002/3, the Crab Nebula was observed with the first two telescopes with the aim to verify the performance of the instrument. Since the object is observed at large zenith angles – beyond $45°$ – the energy threshold is increased and the sensitivity decreased compared to observations near zenith. Nevertheless, the Crab Nebula is clearly visible, even without background subtraction (Fig. 7). The reconstructed energy spectrum [8] agrees well with the spectra measured by other instruments, demonstrating that calibration and effective detection areas of the instrument are well understood (Fig. 8).

Fig. 9 shows the wideband spectra of electromagnetic radiation from the Crab Nebula, from radio wavelengths to 100 TeV gamma rays [7]. I would like to use this spectrum to illustrate some of the mechanisms responsible for gamma ray production. Most likely, all high-energy gamma rays are secondary products generated in interactions of accelerated charged particles – electrons, protons or nuclei. Electrons produce high-energy gamma rays by (Inverse Compton-)upscattering of low-energy quanta (from the radio, infrared or optical domains); depending on the

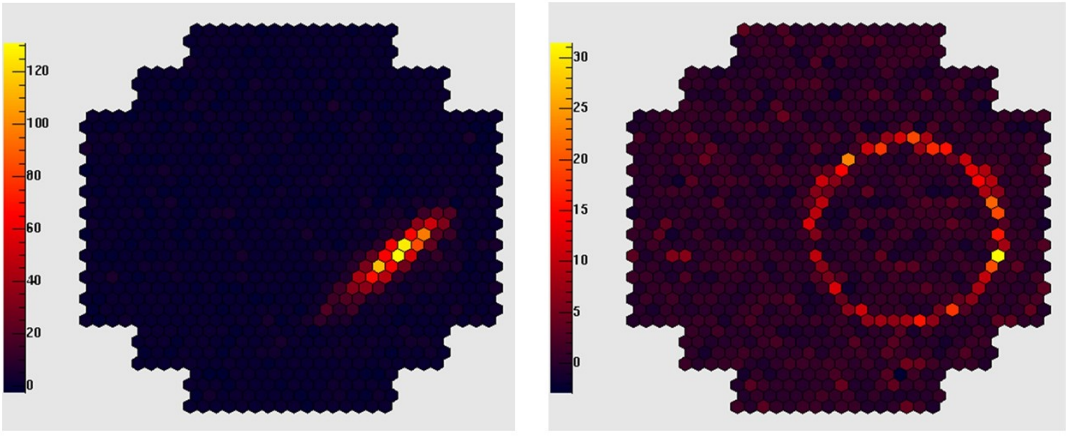

Figure 5: Images of an air shower (left) and of a local muon (right) in the camera of the first H.E.S.S. telescope.

Object	Type	Time [h]	
		2002	2003
1ES 0323+022	AGN		16
Cen X-3	X-ray Binary		48
Crab Nebula	Plerion	39	45
M87	AGN		92
NGC 253	Starburst-Galaxy	28	61
PKS 2005-489	AGN	15	68
PKS 2155-304	AGN	39	162
PSR B1706-44	Pulsar / Plerion		77
RXJ 1713.7-3946	Supernova-Remnant		77
SN 1006	Supernova-Remnant		198
Sgr A East	Galactic Center		42
TeV J1915.2+1147	Unident. TeV Source		27
Vela SNR	Supernova-Remant		43
Others		58	60
Total		**179 h**	**1016 h**
No. of events		**74 M**	**644 M**

Figure 6: H.E.S.S. data samples from 2002 and 2003.

kinematic regime, almost the entire energy of an electron can be transfered to the gamma ray. In the ever-present magnetic fields, electrons also produce synchrotron radiation, which usually manifests itself from radio to X-ray energies. Inverse-Compton (IC) scattering and synchrotron radiation are related processes; in the first case the electron absorbs a regular target photon and emits a new photon, in the second case it interacts with a virtual target photon of the magnetic field. The rate of IC energy losses of primary electrons is governed by the energy density of the target photon fields, the rate of synchrotron losses by the energy density in the magnetic fields (which provide virtual target photons). Under normal interstellar conditions, with fields of a few μG and the cosmic microwave background as the dominant radiation field, the energy densities of the two target components and hence the IC and synchrotron losses are about equal, and in a νF_ν-plot such as Fig. 9 one finds synchrotron and IC components at the same intensity. For the Crab Nebula, the synchrotron energy losses are about three orders of magnitude higher than the IC losses, indicating a high magnetic field (around 160 μG) (e.g. [7, 9] and refs. given there). Synchrotron intensities are in fact so high that synchrotron photons serve as an additional target for the IC process, enhancing VHE gamma ray rates.

Under normal interstellar conditions, an electron population will produce a synchrotron energy flux roughly equivalent to the VHE gamma ray energy flux; the other potential source of VHE gamma rays, proton acceleration followed by proton interactions, π^0 production and decay, will on the other hand not generate significant X-rays, except

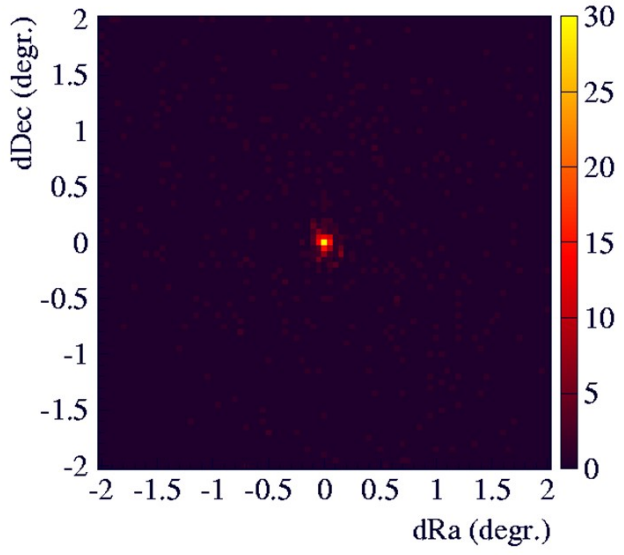

Figure 7: Distribution of reconstructed shower directions relative to the direction to the Crab Nebula, before background subtraction, for an early data set.

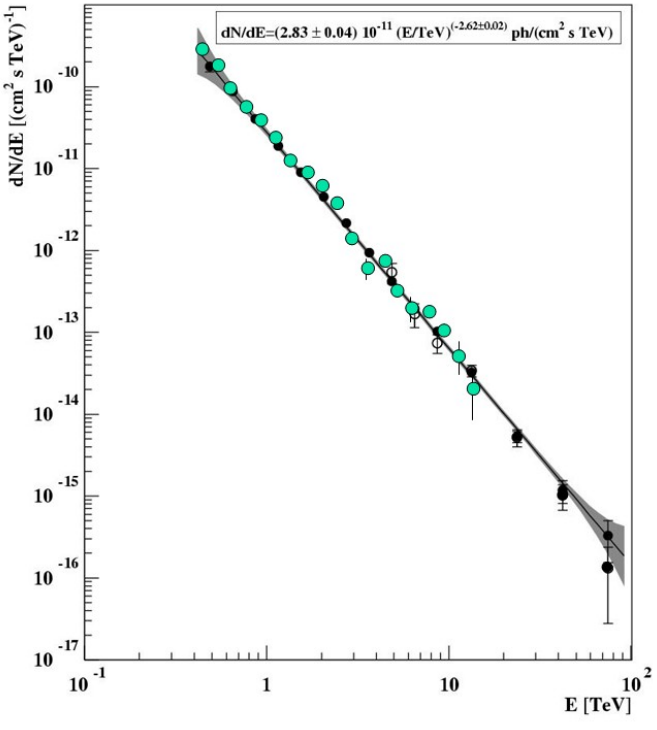

Figure 8: Spectrum of the Crab Nebula as measured by H.E.S.S. (open circles) compared to HEGRA data [7](full circles, shaded region).

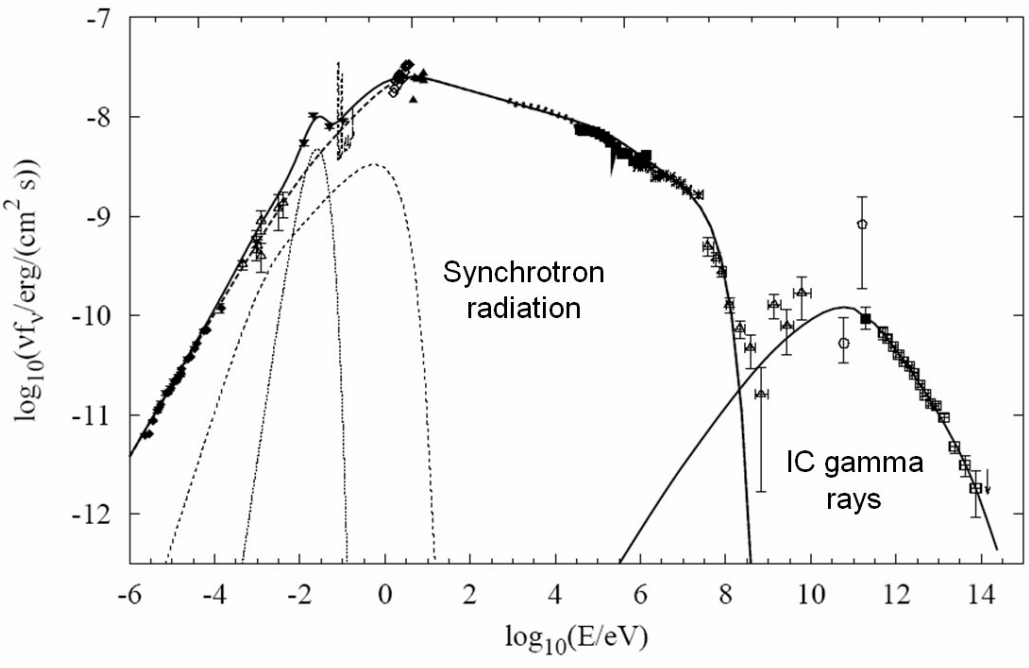

Figure 9: Wideband spectrum of radiation from the Crab Nebula [7]. The quantity $\nu f_\nu \sim E^2 \mathrm{d}N/\mathrm{d}E$ describes the energy flux per logarithmic interval of the spectrum.

through higher-order processes such as gamma-ray pair production or electrons generated in muon decays. Wideband spectra and in particular the X-ray component are therefore crucial in identifying the nature of the primary population of accelerated particles.

3. Gamma emission by supernova remnants

Almost 100 years after the 1912 discovery of cosmic rays by V. Hess the origin and acceleration mechanisms of the high-energy particles are still under dispute. Supernova remnants (SNRs) have long been suspected as the source of cosmic rays, but conclusive experimental evidence is still lacking. Diffusive shock acceleration in supernova shock fronts proceeds as follows (see e.g. [10–12] and refs. given there): through diffusion in the random magnetic fields, particles are contained near the shock and may cross the shock several times, increasing their energy with each crossing by a small amount $O(\beta_{shock})$ when their velocities are isotropised in the new frame. In a process that may take thousands of years, particles can be accelerated up to 10^{14} to 10^{15} eV; the maximum energy is defined by the Larmour radius, which at some point exceeds the size of the shock, and possibly by the age of the supernova remnant. Since in each iteration there is a certain chance that particles diffuse out of the shock region and are swept downstream of the shock, a power law $\mathrm{d}N/\mathrm{d}E \sim E^{-\Gamma}$ with $\Gamma = 2.0...2.2$ emerges. Taking into account the energy-dependent diffusion out of the Galaxy, one can reproduce the observed $E^{-2.7}$ spectrum of cosmic rays below the knee. The acceleration process is nonlinear – the accelerated particles excite plasma waves which in turn help to confine the particles – and reaches high efficiency; well over 10% of the kinetic energy of the supernova explosion may end up in high-energy cosmic rays.

Supernova remnants in the Galactic plane, as likely accelerators of cosmic rays and predicted TeV sources, are obviously a prime target for southern instruments, but already first data taken with the H.E.S.S. instrument on the supernova SN 1006 puzzled the community [13].

TeV gamma ray emission from one of the lobes of the SN 1006 remnant was detected by the first CANGAROO

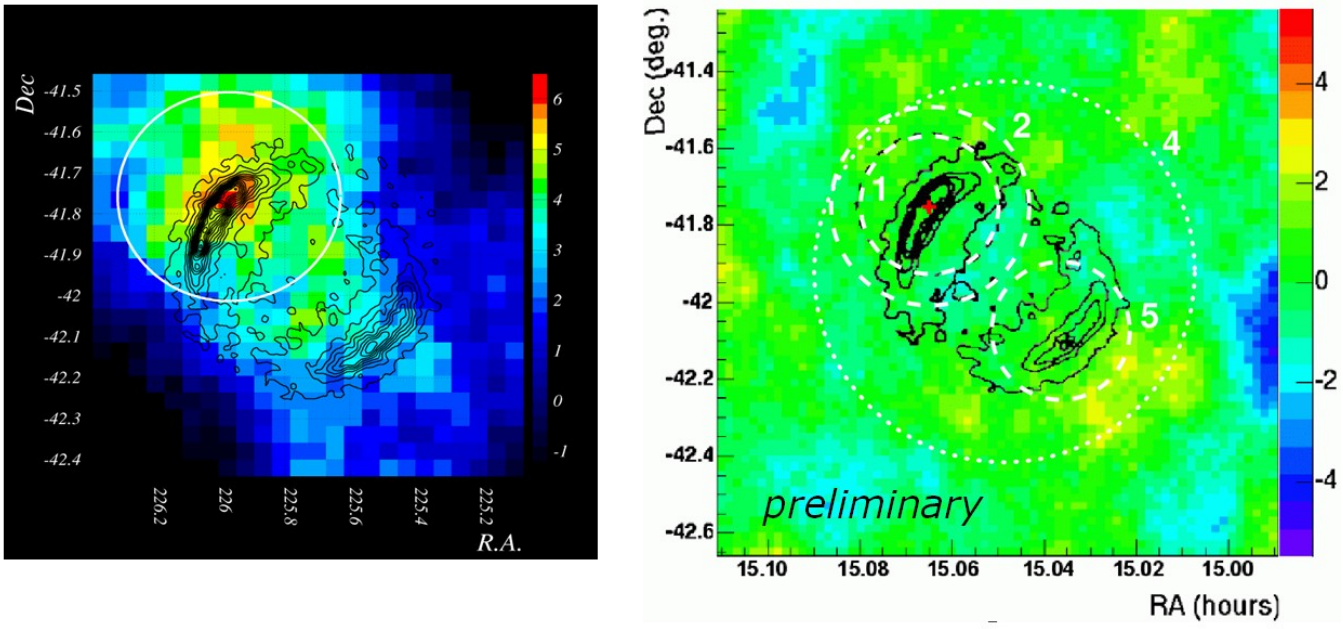

Figure 10: Left: CANGAROO sky map of the region around SN 1006, showing TeV emission from the north-west region of the shell. Right: H.E.S.S. sky map of the region, showing the excess significance as a function of source position. Black lines indicate X-ray contours, circle (2) the CANGAROO hotspot and circle (1) the H.E.S.S. psf.

(3.8 m) telescope, reported in 1998 [14] (Fig. 10, left). Follow-up observations with the CANGAROO II telescope resulted in a detection reported at the ICRC conference in 2001 [15]. The combined X-ray and TeV spectra can be modeled as synchrotron and IC emission of electrons with energies up to 100 TeV in a low (4 μG) magnetic field [16], which would imply an electron origin of the VHE gamma rays, leaving little space for a π^0 decay component which would identify the source as a proton accelerator.

The H.E.S.S. collaboration, both with data from the first telescope alone, and using later multi-telescope data, find no indication for significant TeV emission in the entire SN 1006 field of view (Fig. 10, right); upper limits are derived for the original CANGAROO hotspot assuming both the CANGAROO and the (better) H.E.S.S. point spread function, and for the remnant as a whole. Upper flux limits (Fig. 11) are well below the CANGAROO flux and also below the flux reported for a tentative detection with the HEGRA CT1 telescope at higher energy [17]. In addition to SN 1006, several other claims for TeV emission from southern sources could not be confirmed in H.E.S.S. observations. H.E.S.S. results concerning northern sources are in good agreement with previous data – the flux and spectrum of the Crab Nebula is reproduced, the AGN Mkn 421 was detected and exhibits a cutoff in the TeV region [18], the AGN Mkn 501 was not seen during a very short exposure, but neither was it detected in concurrent observations by VERITAS [19] – and the discrepancies concern in particular southern CANGAROO sources. The main findings are summarized in Table I.

In this situation, one obviously needs to ask if H.E.S.S. data can be trusted at this early stage of the experiment. Facing the non-confirmation of several "classical" southern sources, which was already evident in the data from the first H.E.S.S. telescope taken in 2002, the H.E.S.S. collaboration has spent almost two years scrutinizing their data. Telescope pointing has been checked on a run-by-run basis using the currents induced in the camera PMTs by stars and is understood to better than 20". The absolute sensitivity was verified using the very clean muon rings [21]. Distributions of image parameters were checked against simulations for the Crab and PKS 2155-304 data and excellent agreement is found for the width and length of gamma-ray images, and for the angular distribution with respect to the source [22]. Trigger rates of cosmic rays are well reproduced by the simulations [4]. These simulations

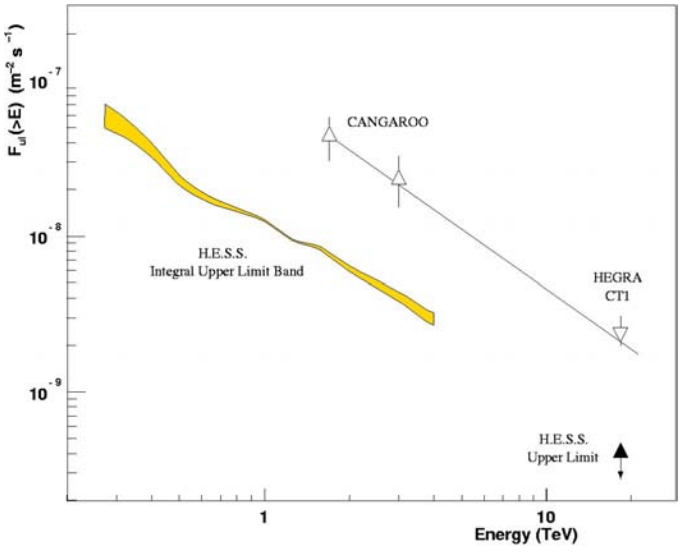

Figure 11: H.E.S.S upper limits on the integral flux from the location of the CANGAROO hotspot, with an integration region corresponding to the CANGAROO psf (preliminary).

Object	**Classification**	**H.E.S.S. result**
PSR 1706-44	A	not detected at level of the old flux
Vela	C	not detected at level of the old flux
SN 1006	B	not detected at level of the old flux
RXJ 1713	B+	20 σ detection, spectrum & flux not incompatible
Gal. center		10 σ detection, spectrum differs
NGC 253	B	not detected at level of the old flux
PKS 2155	B	45 σ detection, spectrum and flux compatible

Table I H.E.S.S. results concerning southern TeV sources detected previously by other instruments. The 'classification' refers to [20], "A" is a solid confirmed detection, "B" is solid, but not confirmed, and "C" implies a somewhat marginal detection.

account for all details of the optical system and of the trigger electronics and recording electronics. Two completely independent analysis chains are used, starting with an independent calibration of pixel amplitudes and identification of problematic or dead pixels [23]. One chain uses the classical Hillas parameterization of shower images, followed by a geometrical reconstruction of the shower axis [22]. Based on the measured impact point, light intensities are converted into energies and spectral data points are derived. The other chain used a full model of Cherenkov light emission by the shower to directly fit the observed pixel intensities in terms of shower parameters [24]. Rather than deriving flux values for energy bins, the counts in individual energy bins are fit using a spectral model, accounting for the resolution function of the instrument and the resulting smearing of the spectrum. These widely different approaches give results which are in agreement. Together with numerous other checks, these procedures make the H.E.S.S. collaboration very confident in their data quality.

The only explanation consistent with the SN 1006 data of the three experiments is a time variation of the flux on a scale of years; however, given the size of the remnant and its structures, such a rapid variation would be surprising. Also, very high fields of order mG would be required to cool an electron population quickly enough. Further data in the X-rays and new TeV data from CANGAROO III will hopefully resolve this puzzle. Models for the TeV emission of SN 1006 can accommodate a lower flux [25]: magnetic fields around 100 μG lower the electron density

required to explain the detected X-rays and thereby lower the predicted IC flux below the detection limits. Hadronic contributions can be suppressed by assuming a low ambient interstellar gas density (0.1 cm^{-3}), which is consistent with all observations, and which, since it enters both in the proton injection rate in the shock and in the number of target protons to produce gamma rays, results in a much lower gamma ray flux than that predicted given the canonical density of 1 cm^{-3} [26].

The second classical TeV SNR is RX J1713.7-3946, again first detected by CANGAROO as a TeV hotspot coincident with one section of the X-ray SNR shell [27]. Using a single-zone IC model, it is difficult to simultaneously fit the X-ray spectra and the TeV spectra; a low magnetic field results in the correct TeV flux but predicts a harder TeV spectrum than observed [28]. Higher fields would soften the TeV spectra in relation to the X-ray spectra, but also suppress the TeV flux well below the measured flux. In consequence, the CANGAROO collaboration have claimed this as proof for a hadronic origin of the TeV gamma rays, and RX J1713.7-3946 as the first uniquely identified source of nuclear cosmic rays [28]. This interpretation has been questioned [29, 30], e.g. on the grounds that the gamma ray spectrum predicted for a hadronic source violates an EGRET upper limit – an argument which might be circumvented by fine-tuning the proton spectrum and the mix of hadronic and IC gamma rays. A more general argument is that given the highly structured (X-ray) SNR, a single-zone IC model is clearly oversimplified. If the magnetic field is high but has a small filling factor, one can achieve softer TeV spectra, but maintain the high TeV intensity since IC gamma rays are emitted from a much larger volume than the X-rays [31]. However, the parameters required to fit the data – 15 μG in 1% of the space – are a bit uncomfortable; if the shock-compressed fields end up in such a small volume, one might expect higher fields.

RX J1713.7-3946 was one of the prime H.E.S.S. targets, and was detected with high significance [32]. More importantly, for the first time in TeV gamma-ray astronomy, the morphology of the source is resolved: the high sensitivity and good angular resolution of the H.E.S.S. instrument expose a shell structure of the TeV radiation (Fig. 12), demonstrating clearly that the acceleration of high-energy particles is associated with the supernova shock. The intensity is non-uniform along the shell; the most intense regions coincide with the location of the CANGAROO detection. As expected for a hadronic accelerator, the spectrum measured by the H.E.S.S. group follows a power law with photon index $\Gamma \approx 2.2$ (Fig. 13); it is marginally consistent with the steeper CANGAROO spectrum, but a direct comparison is difficult since the H.E.S.S. spectrum refers to the whole remnant, while the CANGAROO spectrum covers only part of the rim. The H.E.S.S spectra favor a hadronic origin of the TeV gamma rays, but definitive statements will have to await further data, allowing a more detailed cross-correlation between the TeV emission profile and both the X-ray features (relevant for IC contributions) and the local structure of the interstellar medium (relevant for hadron interactions).

A key issue in the interpretation of TeV gamma radiation from SNR continues to be the value of the magnetic field. High (average) fields – above some 20 to 50 μG – will suppress IC gamma rays relative to X-rays and will leave only interactions of hadronic cosmic rays as plausible origin of gamma-ray signals. Several authors (e.g. [33–36]) have argued that in fact the narrow structures observed in Chandra images of SN 1006 [37] (Fig. 14) and of Cassiopeia A do require higher fields, which both suppress diffusion of X-ray emitting electrons away from the supernova shock and which result in rapid cooling of the electrons, thereby confining the X-ray emission to the proximity of the shock.

4. Pulsars and pulsar wind nebulae

Another class of objects which has attracted much attention and experimental effort includes pulsars and pulsar-wind driven nebula. In contrast to shock acceleration, particle acceleration in pulsars is based on the electric fields generated by the rotating magnetic dipole. In pulsar wind nebulae, shock acceleration takes place in a second stage in the wind termination shock. The best-studied object of this type is the Crab Nebula.

The pulsar PSR 1706-44 was detected with high significance by the CANGAROO I [38] and II telescopes [39], and was also seen by the Durham group [40]. At a flux of roughly 1/2 of the Crab flux, it was long considered as the southern equivalent of the Crab nebula. As noted by several authors, the high TeV flux is surprising [41, 42], given that the pulsar has a spindown luminosity of about 1% of the Crab pulsar, and the X-ray luminosity of the pulsar

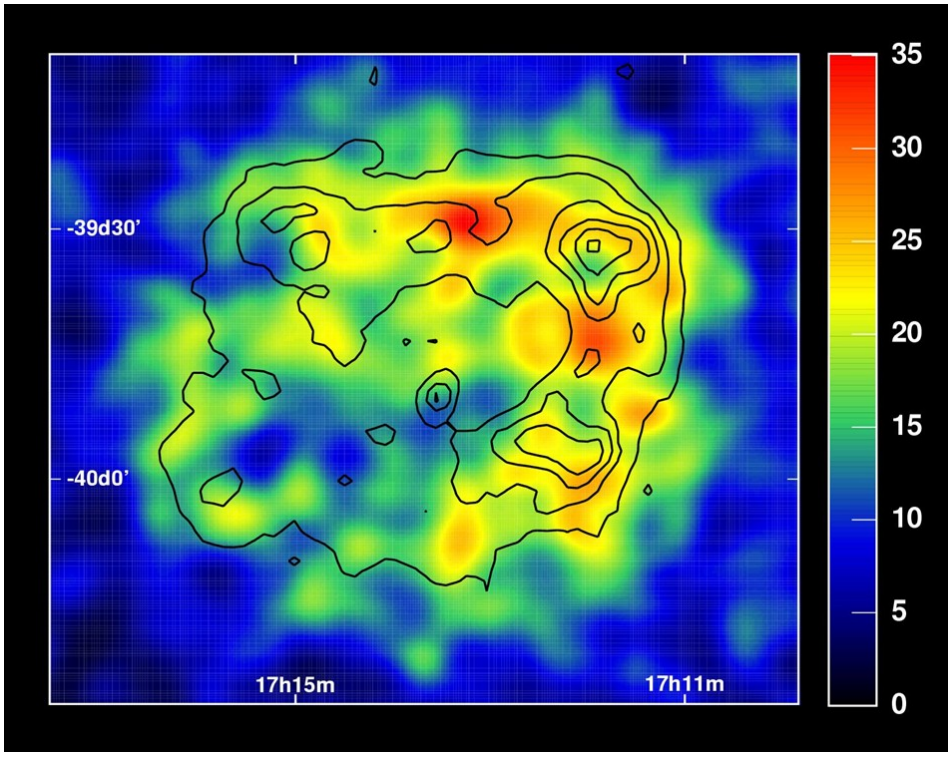

Figure 12: Sky map of RX J1713.7-3946; colors indicate the H.E.S.S. TeV gamma ray flux, contours the X-ray flux.

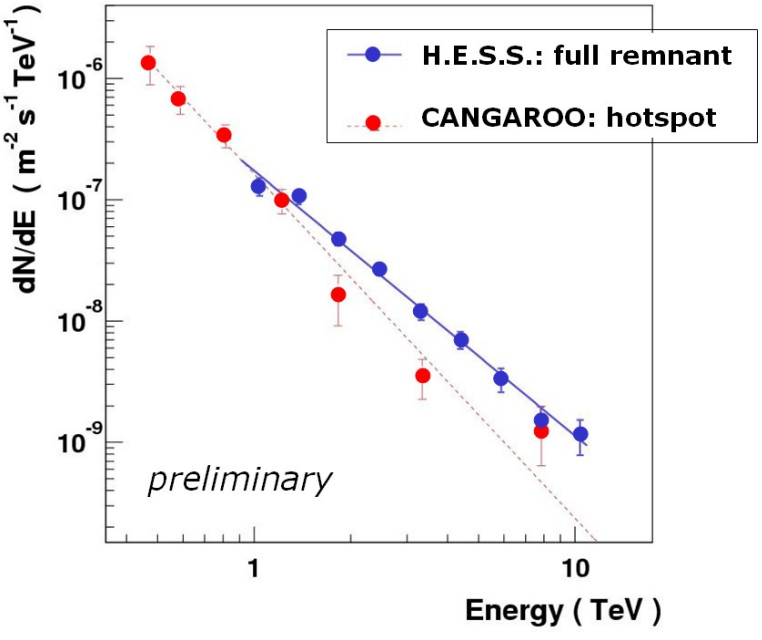

Figure 13: Gamma-ray spectra of RX J1713.7-3946, measured by the H.E.S.S. instrument for the full remnant, and by CANGAROO for the hotspot region.

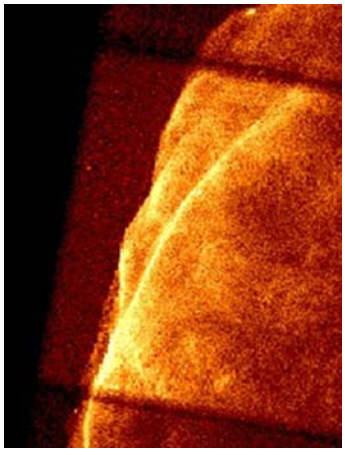

Figure 14: Chandra image of the north-west section of the SN 1006 shell [37].

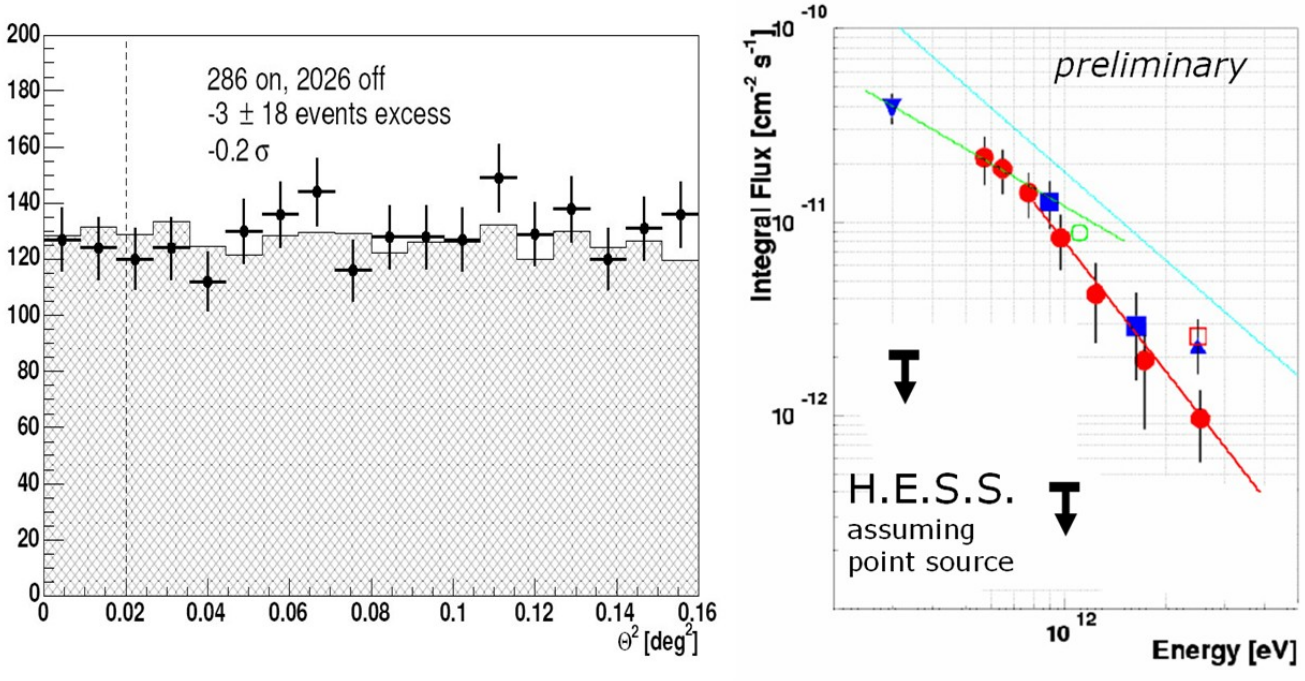

Figure 15: Left: distribution of gamma-ray candidates in the H.E.S.S. data relative to the direction to PSR 1706-44; shaded area shows background estimate. Right: Durham (triangle) and CANGAROO (circles, squares) measurements of the integral flux as a function of threshold energy, and new H.E.S.S. flux limits (preliminary).

wind nebula is only 0.01% of the Crab. Unless one assumes that TeV gamma rays are emitted from a much larger volume than X-rays, the TeV flux cannot be explained in the framework of Inverse Compton scattering models, which predict an emission at a flux level of 10^{-2} to 10^{-3} of the Crab TeV flux [43].

H.E.S.S. data resulting from 14 h of observations with two telescopes during the commissioning phase show no indication of a signal from the direction of PSR 1706-44 (Fig. 15, left). Upper flux limits (Fig. 15, right) are about one order of magnitude below the fluxes reported earlier [44].

However, the original 12σ detection of PSR 1706-44 by CANGAROO also looked very solid. An error in the

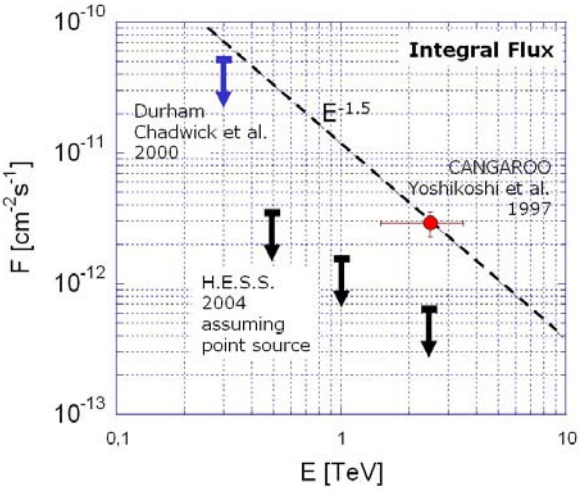

Figure 16: Measurements and limits for the integral flux from the Vela pulsar. The H.E.S.S. limits (preliminary) refer to the (offset) CANGAROO position; similar limits are obtained for the pulsar position.

CANGAROO flux estimate by a factor of 10 seems impossible; while in 1992/3, when the CANGAROO data were taken, the calibration of Cherenkov telescopes was certainly not as well understood and studied as it is nowadays, a flux below the current H.E.S.S. limit could not have been detected with the early CANGAROO telescope. Another explanation is a time dependence; while not really expected for emission from a pulsar nebula, it cannot be excluded from first principles, given the compact size of the PSR 1706-44 nebula. Finally, one could argue that the object may not be a point source; since the H.E.S.S. instrument has a smaller point spread function and integrates over a smaller solid angle, this would reduce the detected flux. Use of a wider source region to match the CANGAROO psf, however, still results in upper limits which are well below the old flux.

A similar situation is observed for Vela. Here, the CANGAROO source [45] seemed offset by 0.13° from the pulsar. H.E.S.S. upper limits (Fig. 16) are again well below the previous flux, both for the pulsar position and the offset position [44]. In this case, however, the original CANGAROO detection is not as strong as for PSR 1706-44, and one has the impression that part of the 5.8σ signal is caused by a dip in the background; also, questions concerning the stability of the analysis were raised in [46].

Compensating for this "loss" of some old sources, the H.E.S.S. collaboration have reported exciting new results, in particular the detection of the pulsar PSR B1259-63 and, in the same field of view, of a new unidentified TeV source.

PSR B1259-63 is a 48 ms pulsar in a highly eccentric orbit around a massive Be star with a disk-like outflow. Every 3.4 years, near periastron, the pulsar crosses the disk and is exposed to strong radiation fields and increased ambient density. Electrons or protons accelerated by the pulsar or by shocks in the wind or stellar outflow will, near periastron, find enhanced targets for the production of TeV gamma rays by the IC mechanism or by hadronic interactions, resulting in a modulation of the TeV gamma-ray flux with the orbital period of the pulsar [47, 48]. The exact pattern of flux variation depends (in the IC scenario) on the relative alignment of pulsar orbit, disk, and viewing direction and could result either in a maximum or a minimum at periastron. CANGAROO has reported upper limits for a section of the orbit far from periastron [48]. In the H.E.S.S data (Fig. 17) the pulsar is detected both before and after periastron, with 9σ and 7σ, respectively [49]. Due to full moon, no data could be taken around periastron, but both the pre- and post-periastron data show a decrease in flux towards periastron, suggesting a flux minimum rather than a maximum. The average flux of PSR B1259-63 is about 7% of the Crab flux (above the 380 GeV threshold), the spectral index is 2.7 ± 0.3(stat). We note that PSR B1259-63 is the first variable galactic TeV source.

Quite a surprise was the discovery of a new steady TeV source 0.6° north of PSR B1259-63; for the first time, two

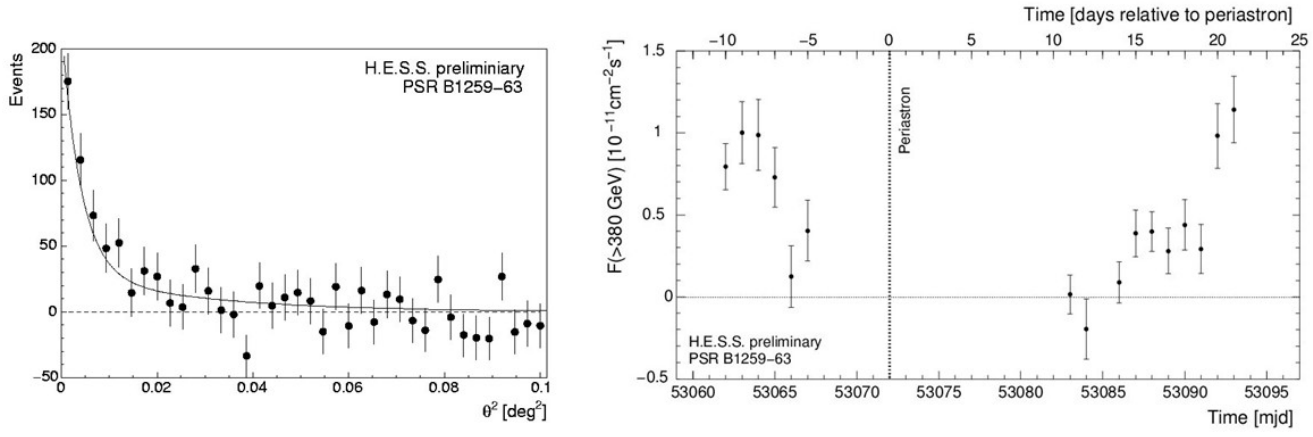

Figure 17: Left: excess of gamma-ray candidates in the H.E.S.S. data relative to the direction to PSR 1259-63. Right: light curve (preliminary).

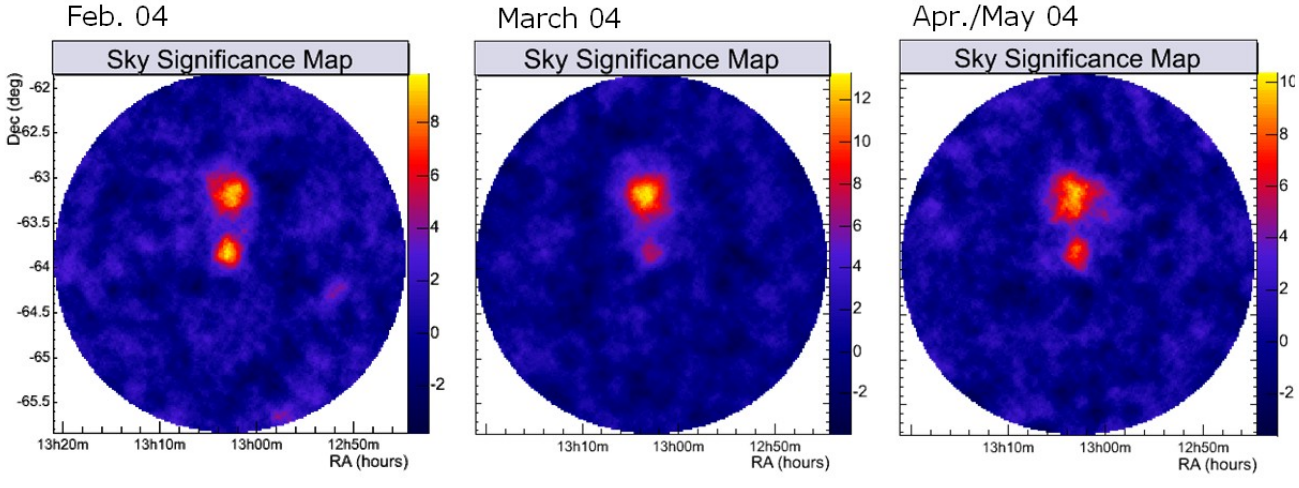

Figure 18: PSR 1269-63 field of view during three observation periods, illustrating the variable emission from the pulsar and the second steady, extended source HESS J1303-631 north of the pulsar.

TeV sources are visible in the field of view of a Cherenkov instrument (Fig. 18). The new source is located at 13^h03^m, $-63.2°$, is highly significant ($\approx 20\sigma$), does not exhibit any significant variability over a period of several months, and is extended at the 0.2° level. The flux corresponds to about 10% of the Crab flux and the spectrum is rather hard, with a photon index $\Gamma \approx 2.2$, see [50]. There is no obvious counterpart at other wavelengths. Since the source is extended, a Galactic location is likely. In its characteristics – extension and hard spectrum – the source matches the northern unidentified HEGRA source [51, 52]. Given that the hard spectrum coincides with expectations for shock acceleration of protons, and given the lack of strong X-ray emission, one might suspect that these sources belong to a new class of cosmic-ray accelerators.

5. The Galactic Center

The Galactic Center provides an environment with many potential TeV sources, ranging from mundane diffuse emission of cosmic rays interacting with the dense (10^3 cm^{-3}) gas to exotic processes such as curvature radiation from the black hole [53] or dark matter (DM) annihilation (e.g. [54, 55] and refs. given there). Recently, the CANGAROO group has reported the detection of TeV gamma rays from the Galactic Center in data taken in 2001 and 2002 [56]. Within the resolution of about 0.2°, the source location is consistent with Sgr A*. The gamma rays exhibit a rather soft energy spectrum, with a photon index $\Gamma = 4.6 \pm 0.5$. The spectrum can be interpreted [56] both in terms of diffuse cosmic-ray-induced emission, or in terms of annihilation of (TeV) DM particles, in the latter case, however, an enhanced density or annihilation cross section is required to explain the relatively high flux. Observations at large zenith angles with the Whipple telescope in the years 1995 through 2003 resulted in a marginal (3.7σ) detection at a threshold of 2.8 TeV [57], with a flux above the extrapolation of the CANGAROO spectrum.

The Galactic Center was also observed with the H.E.S.S. telescopes; data reported here were taken during the commissioning phase with two telescopes. A clear signal from the Galactic Center is visible even without background subtraction (Fig. 19) [58]. In contrast to the CANGAROO data, the H.E.S.S. collaboration find a hard spectrum (Fig. 20), with a spectral index $\Gamma = 2.2 \pm 0.09 \pm 0.15$, clearly inconsistent with the CANGAROO result. The Whipple data point is marginally consistent with the H.E.S.S. spectrum. One should note that the CANGAROO flux is quite high, almost equivalent to the Crab flux above 200 GeV. Given the sensitivity of H.E.S.S., such a signal would have been visible in minutes and could not have been missed. Again – apart from problems with the instrument or the analysis - the only possible explanation is a time dependence of the source, which would favor an origin very near the central black hole. On the other hand, none of the individual experiments sees, within their statistical and systematic errors, indications for significant variability! With its strong variation in night sky brightness across the field of view (Fig. 21), the Galactic Center region is a bit tricky for Cherenkov telescopes; according to simulations, telescope systems such as H.E.S.S. are not significantly affected, but the Whipple group reports that careful software padding to achieve a uniform noise level is crucial for stable results from the single Whipple telescope [57].

The good angular resolution and well-understood telescope pointing allow the H.E.S.S. telescopes to locate the source with a statistical and systematic error of 30" (Fig. 22), representing almost an order of magnitude improvement over the other instruments. The emission region is consistent both with Sgr A* and with the center of Sgr A East. The spectrum can be understood in terms of diffuse emission driven by protons accelerated in the Sgr A East SNR, in analogy to the interpretation of the CANGAROO data but assuming a higher cutoff. Due to the high ambient ISM density, required proton fluxes and energetics are well within reasonable limits. Given that an (exponential) cutoff of the power-law spectrum below 4 TeV is excluded by the data, an interpretation of the H.E.S.S. spectrum by DM annihilation [59, 60] requires DM masses in excess of 12 TeV, a region not favored by SUSY DM models, but also not excluded [61].

6. Summary

The H.E.S.S. telescopes are in full operation since late 2003 and perform according to specifications, allowing to explore sources down to 1% of the Crab flux and below. Initial data have provided exciting results, including the first image of a supernova remnant where the shell is resolved at TeV energies, and discoveries of new sources. More results will become public in the near future. An expansion of the H.E.S.S. telescope system is under discussion; a promising option is to add a large telescope at the center of the current H.E.S.S. array (Fig. 23), which would expand the energy range to lower energies when used in stand-alone mode, and which would provide improved rejection of hadronic backgrounds when operated in coincidence with the four H.E.S.S. Phase I telescopes, due to its well-defined high-intensity shower image.

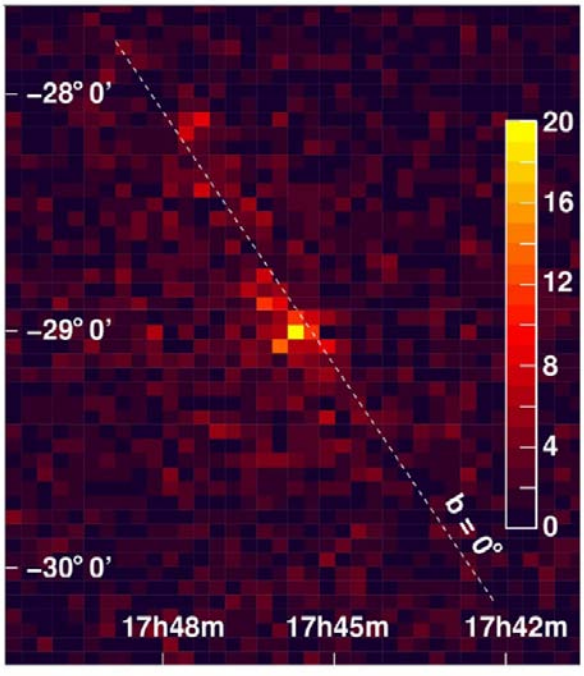

Figure 19: H.E.S.S. sky map of the Galactic Center region, with tight cuts for selection of gamma-ray candidates, before background subtraction.

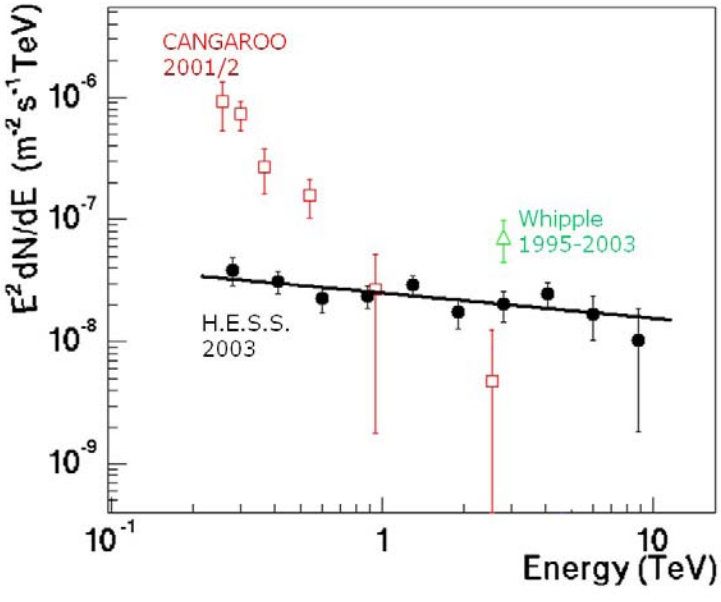

Figure 20: TeV energy spectra of the Galactic Center source as reported by the CANGAROO, Whipple and H.E.S.S. experiments.

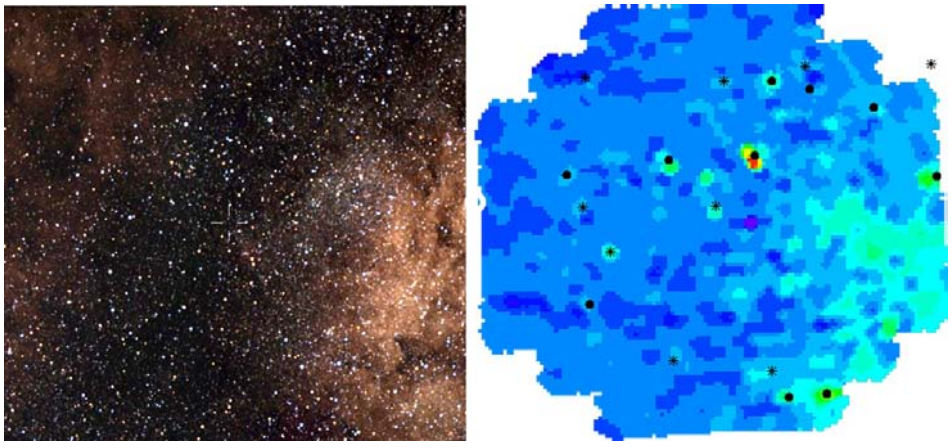

Figure 21: Left: sky image of the Galactic Center region, corresponding roughly to the field of view of the H.E.S.S. cameras. Right: PMT currents, shown as a function of location on the sky, for the Galactic Center. Currents vary by a factor 3 across the field of view of the camera.

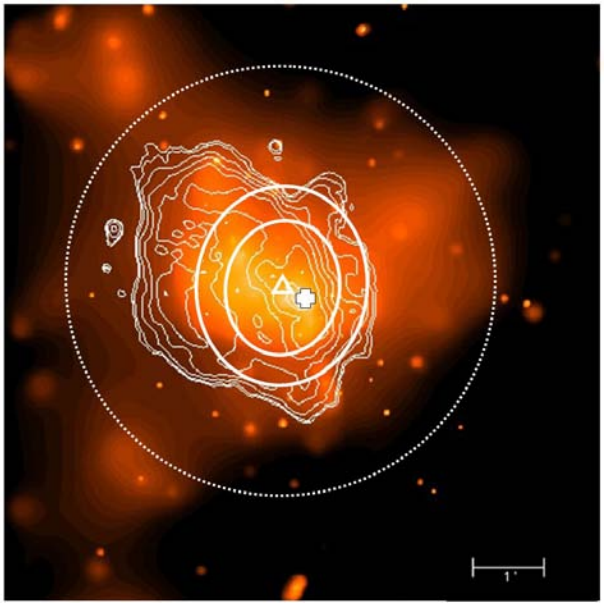

Figure 22: H.E.S.S. localization of the Galactic Center source indicated on a Chandra sky map; the triangle shows the best location, the full circles the 68% and 95% confidence regions, and the dotted circle the upper limit on the rms source size. The cross is Sgr A*; the scale bar indicates 1'.

7. Acknowledgement

The support of the Namibian authorities and of the University of Namibia in facilitating the construction and operation of H.E.S.S. is gratefully acknowledged, as is the support by the German Ministry for Education and Research (BMBF), the Max Planck Society, the French Ministry for Research, the CNRS-IN2P3 and the Astroparticle Interdisciplinary Programme of the CNRS, the U.K. Particle Physics and Astronomy Research Council (PPARC), the IPNP of the Charles University, the South African Department of Science and Technology and National Research Foundation, and by the University of Namibia. We appreciate the excellent work of the technical support staff in

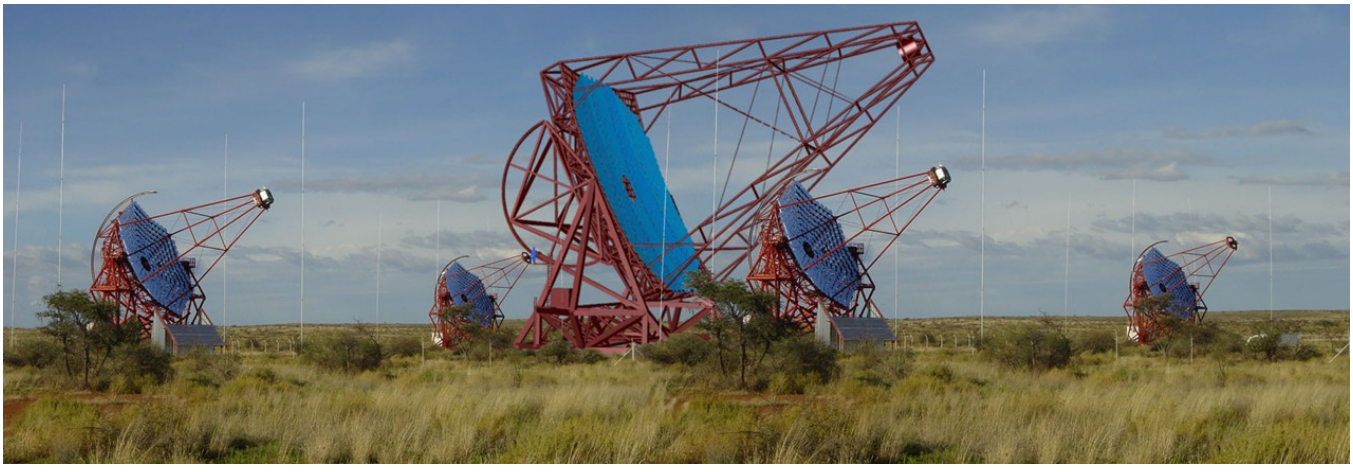

Figure 23: Photo montage showing a scenario for the future expansion of the H.E.S.S. telescope system, with a big dish at the center of the H.E.S.S. Phase I telescope array.

Berlin, Durham, Hamburg, Heidelberg, Palaiseau, Paris, Saclay, and in Namibia in the construction and operation of the equipment.

References

[1] Bernlöhr, K. et al., Astropart. Phys. **20**, 111 (2003)
[2] Cornils, R., et al., Astropart. Phys. **20**, 129 (2003)
[3] Vincent, P., et al., Proc. 28th Int. Cosmic Ray Conf., Tsukuba, 2003, Univ. Academy Press, 2887
[4] Funk, S., et al., Astropart. Phys., in press, astro-ph/0408375 (2004)
[5] Aye, K.M., et al., Proc. 28th Int. Cosmic Ray Conf., Tsukuba, 2003, Univ. Academy Press, 2879
[6] Weekes, T.C., et al., ApJ **342**, 379 (1989)
[7] Aharonian, F., et al., ApJ **614**, 897 (2004)
[8] Masterson, C., et al., submitted to Proc. of the Int. Symp. of High Energy Gamma Ray Astronomy, Heidelberg, 2004
[9] Atoyan, A.M., Aharonian, F.A., MNRAS bf 278, 525 (1996)
[10] Drury, L., Space Sci. Rev. **99**, 329 (2001)
[11] Berezkho, E.G., Völk, H.J., A&A **357**, 183 (2000)
[12] Berezkho, E.G., Ellison, D.C., ApJ **526**, 385 (1999)
[13] Masterson, C., Proc. 28th Int. Cosmic Ray Conf., Tsukuba, 2003, Univ. Academy Press, 2323
[14] Tanimori, T., et al., ApJ **497**, L25 (1998)
[15] Hara, S., et al., Proc. 27th Int. Cosmic Ray Conf., Hamburg, 2001
[16] Tanimori, T., et al., Proc. 27th Int. Cosmic Ray Conf., Hamburg, 2001
[17] Vitale, V., Proc. 28th Int. Cosmic Ray Conf., Tsukuba, 2003, Univ. Academy Press, 2389
[18] Horns, D., submitted to Proc. of the Int. Symp. of High Energy Gamma Ray Astronomy, Heidelberg, 2004
[19] Krennrich, F., priv. comm.
[20] Weekes, T.C., Proc. 28th Int. Cosmic Ray Conf., Tsukuba, 2003, Univ. Academy Press, 1
[21] Leroy, N., et al., Proc. 28th Int. Cosmic Ray Conf., Tsukuba, 2003, Univ. Academy Press, 2895
[22] Benbow, W., submitted to Proc. of the Int. Symp. of High Energy Gamma Ray Astronomy, Heidelberg, 2004
[23] Aharonian, F., et al. (H.E.S.S. Collaboration), Astropart. Phys. **22** 109 (2004)
[24] de Naurois, M., et al., Proc. 28th Int. Cosmic Ray Conf., Tsukuba, 2003, Univ. Academy Press, 2907

[25] Völk, H.J., priv. comm.
[26] Drury, L.O., Aharonian, F.A., Völk, H., A&A **287**, 959 (1994)
[27] Muraishi, H., et al., A&A **354**, L57 (2000)
[28] Enomoto, R., et al., Nature **354**, 823 (2002)
[29] Reimer, O., Pohl, M., A&A **390**, L43 (2002)
[30] Butt, Y.M., et al., Nature **418** 499 (2002)
[31] Lazendic, J.S., et al., ApJ **602**, 271 (2004)
[32] Aharonian, F.A., et al., Nature **432**, 75 (2004)
[33] Vink, J., Laming, J.M., ApJ **584**, 758 (2003)
[34] Berezhko, E.G., Ksenofontov, L.T., Völk, H.J., A&A **412**, L11 (2003)
[35] Berezhko, E.G., Völk, H.J., A&A **419**, L27 (2004)
[36] Yamazaki, R., et al., A&A **416**, 595 (2004)
[37] Bamba, A., et al., ApJ **589**, 827 (2003)
[38] Kifune, T., et al., ApJ **438**, L91 (1995)
[39] Kifune, T., Rapporteur talk at 28th Int. Cosmic Ray Conf., Tsukuba, 2003
[40] Chadwick, P., et al., Astropart. Phys. **9**, 131 (1998)
[41] Kushida, J., Tanimori, T., Kubo, H., Proc. 28th Int. Cosmic Ray Conf., Tsukuba, 2003, Univ. Academy Press, 2493
[42] Aharonian, F.A., Atoyan, A.M., Kifune, T., MNRAS **291**, 162 (1997)
[43] Sefako, R.P., De Jager, O., ApJ **593**, 1013 (2003), and De Jager, O., priv. comm.
[44] Khélifi, B., et al., submitted to Proc. of the Int. Symp. of High Energy Gamma Ray Astronomy, Heidelberg, 2004
[45] Yoshikoski, T. et al., ApJ **487**, L65 (1997)
[46] Dazeley, S.A., et al., Astropart. Phys. **15**, 313 (2001)
[47] Kirk, J., Ball,, L., Skjœraasen, O., Astropart. Phys. **10**, 31 (1999)
[48] Kawachi, A., et al., ApJ **607**, 949 (2004)
[49] Schlenker, S., et al., submitted to Proc. of the Int. Symp. of High Energy Gamma Ray Astronomy, Heidelberg, 2004
[50] Beilicke, M., et al., submitted to Proc. of the Int. Symp. of High Energy Gamma Ray Astronomy, Heidelberg, 2004
[51] Aharonian, F.A., et al., A&A **393**, L37 (2002)
[52] Aharonian, F.A., et al., A&A, in press
[53] Levinson, A., Phys. Rev. Lett. **85**, 912 (2000)
[54] Bergström, L., Ullio, P., Buckley, J.H., Astropart. Phys. **9**, 137 (1998)
[55] Ellis, J., et al., Eur. Phys. J. **C24**, 311 (2002)
[56] Tsuchiya, K., et al., ApJ **606**, L115 (2004)
[57] Kosack, K., et al., ApJ **608**, L97 (2004)
[58] Aharonian, F.A., et al. (H.E.S.S. Collaboration), A&A **425**, L13 (2004)
[59] Horns, D., astro-ph/0408192 (2004)
[60] Bergströ, L., et al., astro-ph/0410359 (2004)
[61] Ellis, J., et al., Phys. Lett. **B565**, 176 (2003)